STUDY OF MHD CORROSION OF RAFM STEEL IN LAMINAR AND TURBULENT PbLi FLOWS IN A WALL-NORMAL MAGNETIC FIELD

Sheida Saeidi,* Sergey Smolentsev, Mohamed Abdou

University of California, Los Angeles, USA
**saeidi@fusion.ucla.edu*

The present study addresses corrosion of RAFM steel in the flowing eutectic alloy PbLi in a special case of the 1-D magnetohydrodynamic Hartmann flow, where the liquid metal flows in a wall-normal magnetic field. For this flow, the effect of a magnetic field on corrosion and transport of corrosion products are studied analytically, using a self-similar mass transfer model, and numerically. The results are presented in the form of the dimensionless mass transfer coefficient (the Sherwood number, Sh) as a function of dimensionless flow parameters, the Reynolds (Re) and the Hartmann (Ha) numbers. In turbulent flows, Sh decreases as Ha increases due to turbulence suppression by a magnetic field. In laminar flows, Sh slightly increases with the magnetic field due to formation of steep velocity gradients at the Hartmann wall. The obtained results are then applied to analysis of corrosion for a family of PbLi blankets.

I. INTRODUCTION

Two important components of a blanket of a fusion power reactor are the liquid breeder/coolant and the steel structure. One candidate combination is lead-lithium (PbLi) eutectic alloy and advanced Reduced Activation Ferritic/Martensitic (RAFM) steel. Implementation of RAFM and PbLi requires material compatibility studies as many questions related to physical/chemical interactions in the RAFM/PbLi system remain open. Moreover, the existing experimental data on corrosion are often contradictive and the underlying physics is not well understood, especially if the PbLi flow is turbulent and strongly affected by the applied magnetic field.

Most of the corrosion studies for the RAFM/PbLi system were performed in the past for purely hydrodynamic flows without a magnetic field, resulting in several correlations for the wall mass loss [1-4] (see also references in Refs. 5 and 6). These studies also suggest that in the range of the flow parameters relevant to PbLi blanket applications, the dominating corrosion mechanism is uniform dissolution of the iron component of steel by the flowing PbLi. This process is known to be fully controlled by mass transfer in the boundary layer. Only a few corrosion studies were performed for flows in a magnetic field typically indicating a strong effect of the magnetic field on corrosion.[5-8] For example, the experimental study of corrosion in a laminar flow in a rectangular duct[8] suggests doubling the corrosion rate once a strong magnetic field is applied.

Ducts of a rectangular cross-section are the key elements of any PbLi blanket, including DCLL (Dual-Coolant Lead-Lithium), HCLL (Helium-Cooled Lead Lithium), WCLL (Water-Cooled Lead-Lithium) and SCLL (Self-Cooled Lead-Lithium) (see references in Ref. 9). In such blankets, corrosion of RAFM walls occurs in the presence of a strong magnetic field, which can be either parallel or perpendicular to the structural wall. In recent theoretical studies,[5] computations were performed for corrosion in MHD laminar flows in a rectangular duct with thin conducting walls of RAFM steel. It was found that corrosion is qualitatively and quantitatively very different between the Hartmann walls (walls perpendicular to the applied magnetic field) and the side walls (walls parallel to the applied magnetic field) because of significant differences in the velocity profile.

The present theoretical study further addresses corrosion in the RAFM/PbLi system focusing on a special case of the 1-D magnetohydrodynamic (MHD) Hartmann flow, where the liquid alloy flows between two parallel steel walls in a wall-normal magnetic field. For this flow, the effect of the magnetic field on corrosion is studied numerically and analytically. Both laminar and turbulent MHD flows are considered.

II. MATHEMATICAL MODEL

The transport model is written here in the boundary-layer approximation, which agrees well with the experimental conditions in almost all experimental studies, where corrosion occurred in long ducts. In such conditions, the diffusion flux in the flow direction can be neglected compared to the convective transport. The governing equations that utilize the boundary-layer approximation for both turbulent and laminar flow include the momentum (1), continuity (2), energy (3), and the mass transfer (4) equations, which are written in terms of the velocity components U and V (m/s), temperature T (K), pressure P (Pa) and iron concentration C (kg/m^3) in the PbLi as follows:

$$\frac{\partial U}{\partial t}+U\frac{\partial U}{\partial x}+V\frac{\partial U}{\partial y}=-\frac{1}{\rho}\frac{\partial P}{\partial x}+\frac{\partial}{\partial y}\left[(\nu+\nu_t)\frac{\partial U}{\partial y}\right]+\frac{1}{\rho}f_{em}, \qquad (1)$$

$$\frac{\partial U}{\partial x}+\frac{1}{y^m}\frac{\partial}{\partial y}\left[y^m V\right]=0, \quad (2)$$

$$\rho C_p\left(\frac{\partial T}{\partial t}+U\frac{\partial T}{\partial x}+V\frac{\partial T}{\partial y}\right)=\frac{1}{y^m}\frac{\partial}{\partial y}\left[y^m(k+k_t)\frac{\partial T}{\partial y}\right], \quad (3)$$

$$\frac{\partial C}{\partial t}+U\frac{\partial C}{\partial x}+V\frac{\partial C}{\partial y}=\frac{\partial}{\partial y}\left[(D+D_t)\frac{\partial C}{\partial y}\right]. \quad (4)$$

The third term f_{em} on the RHS of Eq. (1) is the mean Lorentz force.[10] In the above equations, t is the time, x and y are the coordinates along and across the flow, while ρ, ν, k, σ, and D are the fluid density, kinematic viscosity, thermal conductivity, electrical conductivity and diffusion coefficient of iron in PbLi. The integer parameter m is either 1 (plane channel) or 2 (circular pipe). The counterpart turbulent transport properties are ν_t, k_t, and D_t. The mean PbLi velocity in the channel is U_m, while B_0 is the strength of the applied magnetic field. The turbulent transport properties ν_t, k_t, and D_t are calculated using a special form of the *K*-ε model of turbulence, which takes into account MHD effects.[10] In this model, additional terms that take into account Joule dissipation were included on the RHS of the equations for the turbulent kinetic energy K and the dissipation rate of the kinetic energy ε. The turbulent Prandtl and Schmidt numbers are defined based on recommendations in Ref. 11, typically resulting in magnitudes higher than unity.

Per the assumed corrosion mechanism, the boundary condition for the concentration of iron at the material interface is of the first type: $C_w = C^s$. Based on the experimental data[1-4] this boundary condition might be limited to the velocities of about 0.3 m/s, since erosion can happen at higher velocities. The iron concentration at the flow inlet in all computations is assumed to be zero: $C=0$ at $x=0$. The correlation for saturation concentration is taken from Ref. 5 as follows: $C^s = e^{13.604-12975/T}$, where the saturation concentration is in wppm and the temperature T is in K.

In the corrosion analysis presented in the subsequent sections, we used a numerical code TRANSMAG,[5] which solves Eqs. (1-4) along with the transport equations for K and ε (not shown here).

III. NUMERICAL STUDY OF CORROSION FOR TURBULENT FLOW IN A WALL-NORMAL MAGNETIC FIELD

Effects of a magnetic field on corrosion of RAFM in turbulent PbLi flows in a magnetic field were studied in Ref. 6 for three magnetic field orientations. The magnetic field always suppresses turbulence resulting in lower corrosion rates compared to turbulent hydrodynamic flows. However, the wall-normal magnetic field has the strongest effect on reduction of the corrosion rate due to more intensive suppression of turbulence compared to the spanwise and axial field orientations. For this magnetic field orientation, Fig. 1 shows the wall thinning versus the Hartmann number for the Reynolds numbers from 25,000

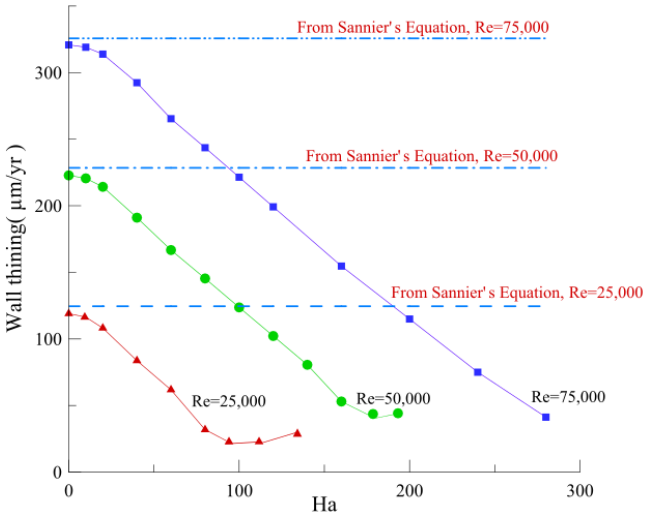

Fig. 1. Comparison of the computed wall thinning with the predictions from Sannier's equation for the case of a wall-normal magnetic field at 500°C.

to 100,000. The dimensionless parameters are constructed in the following way: the Reynolds number $Re = U_m h/\nu$, and the Hartmann number $Ha = B_0 h\sqrt{\sigma/(\nu\rho)}$. Also, we use a dimensionless mass transfer coefficient, the Sherwood number, $Sh = kh/D$, where k is the dimensional mass transfer coefficient and h is the channel width.

As long as the flow is turbulent, the corrosion rate decreases with the magnetic field. Upon reaching the laminar state, the tendency is changed. Namely, the wall thinning starts growing but its increase is less pronounced compared to the fast reduction of the corrosion rate in a turbulent flow. This increase in the corrosion rate in the laminar flow regime is related to formation of the Hartmann layer and associated steep velocity gradients at the Hartmann wall.

The numerical data for the mass loss in the case of a wall-normal magnetic field can be approximated with a dimensionless correlation. It should be mentioned that the widely-used semi-empirical Sannier's correlation [Eq. (5)] for corrosion in hydrodynamic turbulent PbLi flows[3] uses dimensional parameters, such as velocity U_m, temperature T, and channel dimension D_h:

$$v = 8\times10^9 \times Exp\left(\frac{-25690}{1.98T}\right)\times U_m^{0.875}\times D_h^{-0.125}, \mu m/yr. \quad (5)$$

Although Eq. (5) is dimensional, the corrosion data obtained from this correlation for purely hydrodynamic flows can be easily converted to the form of dimensionless Sherwood number Sh_0, which is more appropriate in the context of the present study.

As seen from Fig. 1, Eq. (5) always overestimates corrosion losses compared to the MHD flows. Thus, this

correlation should be corrected to take into account an effect of the magnetic field. In this study, the correlation, which takes into account the effect of a magnetic field, is sought in the following form:

$$Sh - Sh_o = cHa^d . \quad (6)$$

The parameters c and d have been evaluated from the numerical data illustrated in Fig. 1. As a result, the correlation for the Sherwood number with a magnetic field effect takes the following form:

$$Sh = Sh_o - 0.792 \times (Ha^{1.289}) . \quad (7)$$

The new correlation has the same applicability limits as the Sannier's equation itself: velocity 0.01 – 0.3 m/s, temperature 450-550°C, duct dimension 0.005-0.05 m. Maximum magnetic field can be found from $Ha/Re = (Ha/Re)_{cr}$ to assure that the flow is turbulent. The critical value of this parameter for the case of a wall-normal magnetic field is about 1/220 (see Ref. 10). These dimensional limits can also be converted in dimensionless ones: Reynolds number 5,000-100,000, dimensionless temperature 0.81-1.00 (here temperature 500 °C is used as the temperature scale), $Ha < Re/220$.

IV. ANALYTICAL STUDY OF CORROSION FOR THE HARTMANN FLOW

Once the flow becomes laminar at high Ha as explained in Section III, the mass transfer problem can be described with the following mass transfer equation, which is written here in dimensionless form:

$$\widetilde{U}(\widetilde{y})\frac{\partial \widetilde{C}}{\partial \widetilde{x}} = \frac{1}{Pe_D}\frac{\partial^2 \widetilde{C}}{\partial \widetilde{y}^2} . \quad (8)$$

In this equation, the velocity is scaled with the mean bulk velocity: $\widetilde{U} = U/U_m$. The dimensionless concentration is written using the inlet concentration C_0 and the saturation concentration C^s as follows: $\widetilde{C} = (C - C_0)/(C^s - C_0)$. The axial coordinate x and the cross coordinate y are scaled using half of the width of the channel b : $\widetilde{x} = x/b$, $\widetilde{y} = y/b$. The Peclet number for diffusion is $Pe_D = Re \times Sc = U_m b / D$. The initial condition at the inlet is $\widetilde{C} = 0$. The boundary condition at the walls $\widetilde{y} = 0;2$ is $\widetilde{C} = 1$. The velocity profile is the Hartmann velocity profile:

$$\widetilde{U}(\widetilde{y}) = \frac{Ha}{a - tanh(Ha)}\left[1 - \frac{cosh[Ha \times (\widetilde{y} - 1)]}{cosh(Ha)}\right] . \quad (9)$$

In a strong magnetic field, $Ha >> 1$, so that

$$\widetilde{U}(y) = 1 - e^{-Ha \times \widetilde{y}} . \quad (10)$$

Analytical solution to this problem can be obtained in two particular cases denoted Zone I and Zone III. These zones are introduced in association with the development of the concentration boundary layer at the walls of the channel as the liquid proceeds downstream. In Zone I, at the entrance to the channel where corrosion occurs, the thickness of the concentration boundary layer starts from zero and then increases with the axial coordinate as shown in Fig. 3. We assume that within the Zone I, the thickness of the MHD Hartmann layer is higher than the thickness of the concentration boundary layer. The other zone, Zone III, is located at some axial distance downstream from Zone I. Here, opposite to Zone I, the thickness of the concentration boundary layer is higher than the thickness of the Hartmann layer. There is Zone II between Zones I and III, where the MHD boundary layer and the concentration boundary layer are of about the same thickness. However, we don't derive an analytical solution for Zone II due to mathematical complexity for this zone. All three zones are sketched in Fig. 3.

IV.A. Zone I

The first particular case corresponds to the initial section of the boundary layer where the Hartmann layer is thicker than the concentration boundary layer (δ_c). Here, within the boundary layer, the velocity profile can be written as a linear function of $\widetilde{y}$: $\widetilde{U}(\widetilde{y}) = Ha \times \widetilde{y}$. The new dimensionless coordinates are introduced: $\xi = x/b$ and $\eta = y/\delta_c$. As a matter of fact the axial coordinate ξ coincides with $\widetilde{x}$. Using the new coordinates, the original mass transfer problem in this zone near the Hartmann wall can be rewritten as follows:

$$\ddot{\widetilde{C}} + Pe_D Ha\left(\widetilde{\delta}_c^{\,2}\widetilde{\delta}_c'\right)\eta^2\dot{\widetilde{C}} = 0 , \quad (11)$$

$$\eta = 0 : \widetilde{C} = 1 , \qquad \eta = 1 : \widetilde{C} = 0 . \quad (12)$$

Here, the upper "dot" symbol is used for the η derivative, while symbol "prime" is used for ξ derivative. The second of the boundary conditions suggests that at the outer boundary of the concentration boundary layer, the concentration is equal to that at the channel inlet. Equations (11) and (12) allow for a self-similar solution independent of the axial coordinate ξ , providing

$$Pe_D \times Ha \times \tilde{\delta}_c^2 \tilde{\delta}_c' = const_1 . \quad (13)$$

Solving Eq. 13 gives a formula for the thickness of the concentration boundary layer in Zone I:

$$\tilde{\delta}_c(\xi) = const_1^{1/3} \left(\frac{3\xi}{PeHa} \right)^{1/3} . \quad (14)$$

The concentration profile obtained by integration of Eq. 11 is:

$$\tilde{C}(\eta) = -\frac{\eta^2 \Gamma\left(\frac{1}{3}, \frac{Const_1}{3}\right) - \frac{\Gamma\left(\frac{1}{3}, \frac{Const_1 \eta^3}{3}\right)\left(Const_1 \eta^3\right)^{2/3}}{const_1^{2/3}}}{\eta^2 \Gamma\left(\frac{1}{3}\right) - \eta^2 \Gamma\left(\frac{1}{3}, \frac{Const_1}{3}\right)} , \quad (15)$$

where $\Gamma(a)$ is Gamma function and $\Gamma(a,b)$ is incomplete gamma function. The constant $const_1$ entering Eq. (15) needs to be defined. For the self-similar solution defined by Eq. (15) this constant doesn't depend on the flow parameters and hence can be evaluated once by comparing the analytical data with numerical computations. This was found to be 10 to provide expected asymptotic behavior of the concentration profile near the edge of the boundary layer. The thickness of the concentration boundary layer obtained analytically is compared with the numerical computations in Fig. 2. In the numerical computations, the thickness of the boundary layer was defined using a 1% criterion. A good agreement between the analytical and numerical data confirms the adequacy of the analytical approach. Consequently, mass transfer rate J (kg/m^{2}s) expresses as

$$J = k\left(C^s - C^b\right) = -D\frac{\partial C}{\partial y} . \quad (16)$$

Here, the bulk concentration C^b is zero since the finite duct length is considered, where the concentration boundary layer is much thinner than the channel. The mass transfer rate J can also be expressed in a dimensionless form using the Sherwood number as:

$$Sh = \frac{k2b}{D} = -2\frac{\partial \tilde{C}}{\partial \tilde{y}}\bigg|_{\tilde{y}=0} . \quad (17)$$

The analytical solution for Sh in Zone I is :

$$Sh = \frac{2 \times 3^{2/3}}{\Gamma\left(\frac{1}{3}\right) - \Gamma\left(\frac{1}{3}, \frac{10}{3}\right)} \left(\frac{3\xi}{Pe_D Ha} \right)^{-1/3} . \quad (18)$$

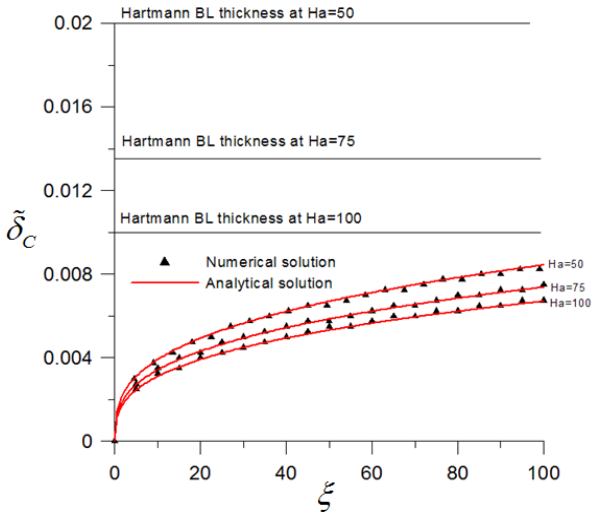

Fig. 2. Comparison for the thickness of the concentration boundary layer in the Zone I between analytical and numerical solutions at $Pe_D = 10^8$.

IV.B. Zone III

The second particular case corresponds to the section of the boundary layer, where the concentration boundary layer is thicker than the Hartmann layer. In this Zone III, the velocity profile can be approximated as $\tilde{U}(\tilde{y}) = 1$.

The mass transfer problem is governed by:

$$\ddot{\tilde{C}} + Pe_D Ha\left(\tilde{\delta}_c \tilde{\delta}_c'\right)\eta \dot{\tilde{C}} = 0 , \quad (19)$$

$$\eta = 0 : \tilde{C} = 1 \quad ,$$

$$\eta = 1 : \tilde{C} = 0 . \quad (20)$$

A self-similar solution to this problem is also possible providing

$$Pe_D \times \tilde{\delta}_c \tilde{\delta}_c' = const_3 . \quad (21)$$

Integrating Eq. (21) results in the following formula for the thickness of the concentration boundary layer:

$$\tilde{\delta}_c(\xi) = \sqrt{\tilde{\delta}_c^2(\xi_o) + \frac{2const_3}{Pe_D}(\xi - \xi_o)} . \quad (22)$$

Once condition (21) is satisfied, the self-similar solution for the problem can be found as follows:

$$\tilde{C}(\eta) = 1 - erf\left(\frac{\sqrt{Const_3}\eta}{\sqrt{2}} \right) \Big/ erf\left(\frac{\sqrt{Const_3}}{\sqrt{2}} \right) , \quad (23)$$

where erf stands for error function.

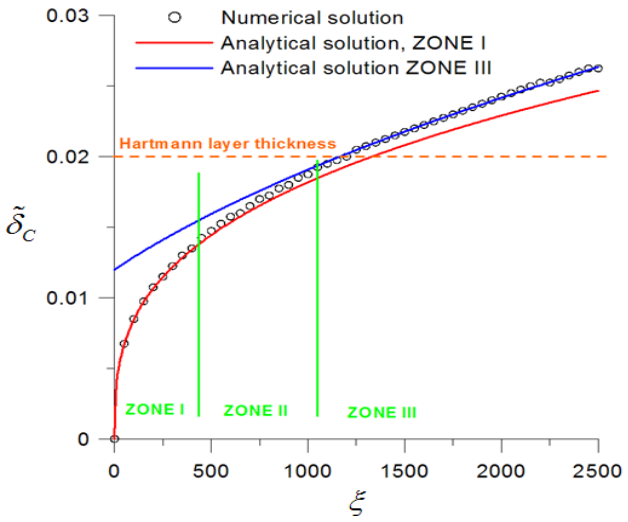

Fig. 3. Comparison between the numerical solution and the analytical solutions for Zones I and III for Ha=50, Pe_D=10^8.

In Eqs. (22) and (23), $const_3$ and ξ_o and $\tilde{\delta}_c(\xi_o)$ need to be defined. The constant was found in the same way as described above for the Zone I. The numerical value of this constant is $const_3 = 11$. The two other parameters can be found from the numerical solution. The coordinate ξ_o was chosen such that $\tilde{\delta}_c(\xi_o) = 1/Ha$, *i.e.* at $\xi = \xi_o$ the thickness of the concentration boundary layer is equal to the Hartmann layer thickness. The analytical solution for the Sherwood number for Zone III is:

$$Sh = \frac{2\sqrt{\frac{22}{\pi}}}{erf\left(\sqrt{\frac{11}{2}}\right)}\left(\tilde{\delta}_C^2(\xi_0) + \frac{22}{Pe_D}(\xi - \xi_0)\right)^{-1/2}. \quad (24)$$

Figure 3 illustrates the obtained data for Zone I, II and III. In Zones I and III, there is a very good agreement between the analytical solution and the numerical computations. In Zone II, both analytical solutions start deviating from the numerical data. In Zone II, which is located between Zones I and III, the thickness of the concentration boundary layer is comparable with the thickness of the Hartmann layer so that the full formula for the velocity profile Eq. (9) or Eq. (10) should be applied. This complicates, however, deriving an analytical solution in Zone II, so that we recommend numerical computations for this zone. As alternative, either Zone I or Zone III solution can be used in Zone II since, as seen from Fig. 3, these solutions can provide reasonable accuracy even in Zone II.

Equation (14) can be used to estimate the dimensionless coordinate ξ_* where the concentration boundary layer and the Hartmann layer are of the same thickness:

$$\xi_* = Pe_D/30Ha\,. \quad (25)$$

Correspondingly, for $\xi < \xi_*$ the concentration boundary layer is thinner and for $\xi > \xi_*$ thicker than the Hartmann layer. It is useful to calculate ξ_* for PbLi blankets and then compare it with the dimensionless blanket duct length L/b. Based on this comparison one can decide what sections of the entire blanket length should be treated as Zone I, II or III.

V. APPLICATION TO A PBLI BLANKET

The obtained solutions can be applied to conditions of a PbLi blanket. Two types of PbLi blankets are of interest here. In a SCLL blanket,[12] the liquid metal flows perpendicular to the lines of the plasma-confining (toroidal) magnetic field in long rectangular ducts. The cross-sectional dimension of such a duct is about 0.2 m (b=0.1 m). The length of a PbLi blanket duct is assumed to be 2 m. The PbLi velocity can be around 0.5 m/s. To avoid corrosion problems, the PbLi temperature is typically limited to about 470 °C. In such flows, formation of Hartmann layers occurs at the duct walls perpendicular to the toroidal magnetic field.

In a dual-coolant PbLi (DCLL) blanket[9], corrosion occurs in the thin ~ 2-mm gap between the structural wall and the SiC flow channel insert. The corrosion processes in the gaps perpendicular to the magnetic field can be analyzed using the present theory since the PbLi flow in such a gap is of the Hartmann type. Here, due to a very small gap width and strong flow opposing electromagnetic forces, the velocities are very small, on the order of 1 mm/s. The maximum temperature of PbLi in the DCLL blanket at the interface between the structural wall and the flowing PbLi in the gap is also restricted to about 470°C to guarantee that the corrosion losses are not too high.

The relevant dimensionless parameters, which enter the analytical solution (Hartmann number, Peclet number for diffusion and the dimensionless duct length L/b) along with the dimensionless length ξ_*, for these two PbLi blanket concepts are summarized in Table I. Two blanket scenarios are considered: an inboard (IB) blanket at magnetic field of 10 T and outboard (OB) blanket at 4 T. The physical properties of PbLi used to calculate the flow parameters were taken at 500 °C.

As seen from the table, in the conditions of the DCLL blanket $\xi_* << L/b$ such that over almost entire blanket length the concentration boundary layer at the Hartmann wall is thicker than the Hartmann layer except for a very

short length at the blanket inlet. Therefore the entire blanket should be considered as Zone III.

TABLE I. Evaluation of ξ_* for DCLL and SCLL Blankets:

Parameter	SCLL IB (B=10 T)	SCLL OB (B=4 T)	DCLL IB (B=10 T)	DCLL OB (B=4 T)
Ha	26500	10600	265	106
Pe_D	(6-15) 10^6	(6-15) 10^6	150	150
L/b	20	20	2000	2000
ξ_*	7.5-18.9	18.9-47.2	0.02	0.03

An opposite tendency can be observed for the SCLL OB blanket, where $\xi_* \geq L/b$ such that the concentration boundary layer is always thinner than the Hartmann layer. The entire blanket can be treated as Zone I. In the case of the SCLL IB blanket, the concentration boundary layer is first thinner and then thicker than the Hartmann layer. For the lower velocity range, the transition occurs closer to the blanket inlet, while for the higher velocity range such transition can be observed close to the blanket outlet. Therefore all three zones I, II and III can be present over the SCLL IB blanket length.

ACKNOWLEDGMENTS

This study is supported by the U.S. Department of Energy, Office of Science, Office of Fusion Energy Sciences, under Award Number DE-FG02-86ER52123.

REFERENCES

1. H.U. BORGSDEDT, H.D. RÖHRIG, "Recent Result on Corrosion Behavior of MANET Structural Steel in Flowing Pb-17Li Eutectic," *J. Nucl. Mater.*, **179-181**, 596-598 (1991); http://dx.doi.org/10.1016/0022-3115(91)90158-4.
2. P.F. TORTORELLI, J.H. DEVAN, "Corrosion of Ferrous Alloys Exposed to Thermally Convective Pb-17 at% Li," *J. Nucl. Mater.*, **141-143**, 592-598 (1986); http://dx.doi.org/10.1016/0022-3115(86)90059-0.
3. J. SANNIER, T. FLAMENT, A. TERLAIN, "Corrosion of Martensitic Steels in Flowing Pb17Li," *Proc. 16th Symp. Fusion Technology*, London, UK, 901-905 (1990).
4. W. KRAUSS, J. KONYS, H. STEINER, J. NOVOTNY, Z. VOSS, O. WEDEMEYER, "Development of Modeling Tools to Describe the Corrosion Behavior of Uncoated EUROFER in Flowing Pb-17Li and their Validation by Performing of Corrosion Tests at T up to 550°C," *FZKA 7295*, Forschungszentrum Karlsruhe (2007).
5. S. SMOLENTSEV, S. SAEIDI, S. MALANG, M. ABDOU, "Numerical Study of Corrosion of Ferritic/Martensitic Steels in the Flowing PbLi with and without a Magnetic Field," *J. Nucl. Mater.*, **432**, 294-304 (2011); http://dx.doi.org/10.1016/j.jnucmat.2012.08.027.
6. S. SAEIDI, S. SMOLENTSEV, "Numerical Study of the Effect of a Magnetic field on Corrosion of Ferritic/Martensitic Steel in a Turbulent PbLi Flow," *Magnetohydrodynamics*, **50 (2)**, 109-120 (2014).
7. F. BARBIER, A. ALEMANY, S. MARTEMIANOV, "On the Influence of a High Magnetic Field on the Corrosion and Deposition Processes in the liquid Pb-17Li Alloy," *Fusion Eng. Des.*, **43**, 199-208 (1988); http://dx.doi.org/10.1016/S0920-3796(98)00420-7.
8. R. KRISHBERGS, E. LIGERE, F. MUKTEPAVELA, E. PLATACIS , A. SHISHKO, A. ZIK, "Experimental Studies of the Strong Magnetic Field Action on the Corrosion of RAFM Steels in Pb17Li Melt Flows," *Magnetohydrodynamics*, **45**, 289-296 (2009).
9. S. SMOLENTSEV, N.B. MORLEY, M. ABDOU, S. MALANG, Dual-Coolant Lead-Lithium (DCLL) Blanket Status and R&D Needs, Fusion Eng. Des. In Press (2015); http://dx.doi.org/10.1016/j.fusengdes.2014.12.031.
10. S. SMOLENTSEV, M. ABDOU, N. MORLEY, A. YING, T. KUNUGI, "Application of the k-epsilon Model to Open Channel Flows in a Magnetic Field," *Int. J. Eng. Sci.*, **40**, 693-711 (2002); http://dx.doi.org/10.1016/S0020-7225(01)00088-X.
11. X. CHENG, N.I. TAK, "CFD Analysis of Thermal-Hydraulic Behavior of Heavy Liquid Metals in Sub-Channels," *Nuclear. Eng. Des.*, **236**, 1874-1885 (2006); http://dx.doi.org/10.1016/j.nucengdes.2006.02.001.
12. S. MALANG, R. MATTAS, "Comparison of Lithium and the Eutectic Lead-Lithium Alloy, Two Candidate Liquid Metal Breeder Materials for Self-Cooled Blankets," *Fusion Eng. Des.*, **27**, 399-406 (1995); http://dx.doi.org/10.1016/0920-3796(95)90151-5.